

# Chapter 7

## Image Resampling (*GEOM*)

Raw *IUE* images suffer from spatial distortions introduced by the SEC Vidicon cameras. The electrostatically-focused imaging section of the camera produces a pincushion distortion, while the magnetically-focused readout section produces an S-distortion. Furthermore, the dispersion direction lies at an angle of approximately 45 degrees relative to the image axes and the dispersion function is not linear within the spectral orders. The combination of these effects make the task of spectral extraction and subsequent analysis very difficult. The goal of the *GEOM* module is to create a geometrically-resampled and spatially-rotated image in which the spectral orders are horizontally aligned and the dispersion is linear within each order thus providing an image format that is best suited for scientific analysis. The *GEOM* step operates on the linearized (i.e., photometrically corrected) image (LI).

The NEWSIPS approach to producing a geometrically resampled image (SI) is to construct a vector field that maps each pixel from its instrumental raw space to a geometrically rectified space. For both low- and high-dispersion images, these vectors include corrections for the following effects:

- the displacements between the raw science image and the Intensity Transfer Function (ITF),
- the displacement of the reseau pattern (camera fiducials) in the ITF from its original square grid,
- the rotation of the spectral format to lie along image rows, and
- the small change of scale needed to linearize the dispersion.

In addition to the above corrections common to both dispersions, the vectors applied to low-dispersion SI data include:

- the shift to align the two spectrograph apertures in wavelength space,
- corrections for the spatial deviations (cross-dispersion “wiggles”) in the long-wavelength cameras,

- a correction (detilting) for extended sources to account for the fact that the major axis of the large aperture is not exactly perpendicular to the dispersion direction, and
- shifts in both the wavelength and spatial directions to maintain a fixed starting wavelength and spatial position in the image,
- an adjustment to the LWP data to put the large-aperture data at the top, and
- an adjustment so that both long wavelength cameras provide coverage of the same spectral range.

In addition to the corrections common to both dispersions, the vectors applied to high-dispersion SI data include:

- corrections for the echelle order splaying,
- spatial shifts for proper alignment of the orders to a fiducial location (order registration), and
- corrections for the cross-dispersion wiggles.

Both the corrections common to both dispersions and the dispersion-specific corrections are discussed in more detail in the sections which follow.

## 7.1 Corrections Common to Both Dispersions

### 7.1.1 Measurement of Distortions

#### 7.1.1.1 Mapping of Raw Science Image to ITF Space

The first correction for image distortion maps the science image to the geometric space of the relevant ITF. This correction utilizes the vector displacements (VD) determined for each pixel during the raw image registration step (Chapter 5). These vectors are unique for each science image and can be recovered from the information in the binary table extension to the final VD FITS file.

#### 7.1.1.2 Mapping of ITF Space to Geometrically Rectified Space

Laboratory measured positions of the fiducial marks (reseau) are used to map the distortion of the null-subtracted 20% level of the ITF in order to compensate for the geometric distortions in the ITF images. The faceplate of each camera is etched with a square-grid pattern of 169 reseau marks arranged in 13 rows and 13 columns. The reseau appear on images as occulted areas approximately 2–3 pixels wide, spaced approximately 55 pixels apart for LWP and LWR and 56 pixels apart for SWP. Of the 169 reseau marks embedded in the fiber-optic coupling, approximately 129 fall within the camera target area. According to the

design specifications of the scientific instrument (GSFC System Design Report for the *IUE*, 1976), the placement of the reseau marks in a true square grid is accurate to within  $\pm 0.005$  mm, which corresponds to  $\pm 0.138$  pixels for LWP/LWR and  $\pm 0.14$  pixels for SWP.

In order to refine the true locations of the reseau marks, laboratory measurements were made of the reseau grid on an SEC Vidicon camera which was manufactured about the same time as the *IUE* cameras; therefore, the same deposition mask was used for the reseaux. The work was performed by the Metrology Department at Rutherford Appleton Laboratory (Didcot, U.K.) in late 1990. The measurements were obtained in an X/Y reference frame in millimeters with a demonstrated repeatability of  $\pm 0.003$  millimeters. As a result, it was necessary to derive a scale factor to convert the millimeter measurements to “true” pixel locations for the reseaux. Note that the NEWSIPS true reseau positions may be very different from the positions quoted for IUESIPS. The IUESIPS reseau positions are *not* laboratory measurements, but rather a square grid construct based upon the definitions of a central reseau mark and mean reseau spacing. The NEWSIPS true reseau positions are listed in Tables 7.1–7.6.

The observed positions of the reseau marks are determined per ITF, and the departures of the observed positions from their true locations are used to characterize the geometric distortion of the camera system. A vector field defining the displacement of each pixel in the null-subtracted 20% level of the ITF from geometrically rectified space is derived using a bi-cubic spline interpolation between the reseau marks.

### 7.1.2 Image Rotation

The image rotation is not, strictly speaking, a distortion correction, but rather is an image remapping performed to simplify the extraction of spectral data from the SI. The purpose of the rotation is to align the spectral order(s) horizontally along the geometrically rectified image.

### 7.1.3 Wavelength Linearization

As discussed in Chapter 8.1, the dispersion solutions for the SI are not precisely linear; significant second- and third-order terms are present in both dispersion modes. The nonlinearities which exist in the dispersion solutions for the SI can, if not accounted for, lead to wavelength errors on the order of several Ångstroms (low dispersion) or several kilometers per second (high dispersion) in some regions of the spectrum. Therefore, a remapping of the SI data is necessary to force the dispersion solution onto a linear scale. In low dispersion, the high-order terms for a given camera are quite stable over time and camera temperature (THDA) so that a single third-order correction can be applied to all of the data for a given camera. The same holds true for high dispersion except that individual solutions are applied independently to each echelle order. The derivation of the corrections is discussed in detail in Chapter 8.1.

The form of the low-dispersion linearization correction for each camera is displayed in

Table 7.1: LWP True Reseau Positions in X Direction

	1	2	3	4	5	6	7
1	80.39	135.37	190.32	245.29	300.11	355.10	410.15
2	80.39	135.35	190.26	245.25	300.17	355.11	410.18
3	80.33	135.32	190.32	245.25	300.17	355.10	410.20
4	80.39	135.39	190.33	245.24	300.20	355.18	410.18
5	80.39	135.40	190.32	245.25	300.20	355.15	410.21
6	80.39	135.30	190.26	245.20	300.17	355.09	410.18
7	80.41	135.33	190.33	245.22	300.20	355.15	410.21
8	80.39	135.24	190.26	245.13	300.13	355.07	410.18
9	80.39	135.25	190.25	245.13	300.09	355.09	410.20
10	80.37	135.22	190.22	245.11	300.09	355.10	410.14
11	80.36	135.20	190.18	245.03	300.02	355.00	410.09
12	80.33	135.26	190.24	245.18	300.10	355.13	410.15
13	80.36	135.26	190.22	245.13	300.07	355.10	410.14

	8	9	10	11	12	13
1	465.00	520.00	574.88	629.81	684.67	738.86
2	465.04	520.06	574.88	629.88	684.73	738.93
3	465.04	520.04	574.92	629.84	684.77	739.14
4	465.06	520.06	574.93	629.71	684.76	739.15
5	465.07	520.06	574.99	629.78	684.76	739.25
6	465.03	520.02	574.92	629.70	684.73	739.32
7	465.10	520.10	574.95	629.76	684.67	739.36
8	465.04	520.09	574.91	629.70	684.56	739.29
9	465.03	520.04	574.93	629.70	684.55	739.34
10	465.00	520.04	574.93	629.63	684.52	739.34
11	464.96	519.92	574.81	629.54	684.38	739.32
12	465.04	520.03	574.88	629.70	684.36	739.45
13	465.03	520.03	574.89	629.74	684.51	739.54

Table 7.2: LWP True Reseau Positions in Y Direction

	1	2	3	4	5	6	7
1	60.40	60.32	60.29	60.39	60.32	60.33	60.29
2	115.35	115.22	115.44	115.44	115.39	115.40	115.33
3	170.20	170.21	170.30	170.50	170.30	170.36	170.18
4	225.21	225.22	225.41	225.46	225.41	225.30	225.24
5	280.18	280.13	280.36	280.43	280.32	280.36	280.21
6	335.20	335.13	335.32	335.32	335.30	335.21	335.11
7	390.14	390.07	390.24	390.32	390.22	390.14	390.04
8	445.04	445.09	445.18	445.35	445.29	445.28	445.07
9	500.21	500.09	500.18	500.33	500.17	500.21	500.10
10	555.10	555.13	555.22	555.30	555.25	555.15	554.98
11	610.00	610.07	610.04	610.29	610.15	610.09	609.93
12	664.93	665.05	665.03	665.30	665.14	665.13	664.98
13	719.96	720.15	720.13	720.20	720.04	720.11	719.98

	8	9	10	11	12	13
1	60.36	60.26	60.32	60.30	60.29	60.29
2	115.26	115.29	115.32	115.25	115.22	115.22
3	170.33	170.30	170.33	170.13	170.24	170.17
4	225.30	225.20	225.26	225.17	225.11	225.32
5	280.29	280.20	280.24	280.18	280.25	280.33
6	335.29	335.22	335.21	335.14	335.17	335.29
7	390.18	390.11	390.17	390.06	390.15	390.24
8	445.22	445.11	445.18	445.17	445.14	445.29
9	500.15	500.13	500.25	500.13	500.09	500.22
10	554.98	555.04	555.18	555.03	555.06	555.29
11	610.09	609.99	610.03	609.99	609.92	610.17
12	665.04	665.00	664.93	664.89	664.92	665.13
13	720.04	719.93	719.87	719.93	719.98	720.20

Table 7.3: LWR True Reseau Positions in X Direction

	1	2	3	4	5	6	7
1	80.39	135.37	190.32	245.29	300.11	355.10	410.15
2	80.39	135.35	190.26	245.25	300.17	355.11	410.18
3	80.33	135.32	190.32	245.25	300.17	355.10	410.20
4	80.39	135.39	190.33	245.24	300.20	355.18	410.18
5	80.39	135.40	190.32	245.25	300.20	355.15	410.21
6	80.39	135.30	190.26	245.20	300.17	355.09	410.18
7	80.41	135.33	190.33	245.22	300.20	355.15	410.21
8	80.39	135.24	190.26	245.13	300.13	355.07	410.18
9	80.39	135.25	190.25	245.13	300.09	355.09	410.20
10	80.37	135.22	190.22	245.11	300.09	355.10	410.14
11	80.36	135.20	190.18	245.03	300.02	355.00	410.09
12	80.33	135.26	190.24	245.18	300.10	355.13	410.15
13	80.36	135.26	190.22	245.13	300.07	355.10	410.14

	8	9	10	11	12	13
1	465.00	520.00	574.88	629.81	684.67	738.86
2	465.04	520.06	574.88	629.88	684.73	738.93
3	465.04	520.04	574.92	629.84	684.77	739.14
4	465.06	520.06	574.93	629.71	684.76	739.15
5	465.07	520.06	574.99	629.78	684.76	739.25
6	465.03	520.02	574.92	629.70	684.73	739.32
7	465.10	520.10	574.95	629.76	684.67	739.36
8	465.04	520.09	574.91	629.70	684.56	739.29
9	465.03	520.04	574.93	629.70	684.55	739.34
10	465.00	520.04	574.93	629.63	684.52	739.34
11	464.96	519.92	574.81	629.54	684.38	739.32
12	465.04	520.03	574.88	629.70	684.36	739.45
13	465.03	520.03	574.89	629.74	684.51	739.54

Table 7.4: LWR True Reseau Positions in Y Direction

	1	2	3	4	5	6	7
1	60.40	60.32	60.29	60.39	60.32	60.33	60.29
2	115.35	115.22	115.44	115.44	115.39	115.40	115.33
3	170.20	170.21	170.30	170.50	170.30	170.36	170.18
4	225.19	225.22	225.41	225.46	225.41	225.30	225.24
5	280.18	280.13	280.36	280.43	280.32	280.36	280.21
6	335.20	335.13	335.32	335.32	335.30	335.21	335.11
7	390.14	390.07	390.24	390.32	390.22	390.14	390.04
8	445.04	445.09	445.18	445.35	445.29	445.28	445.07
9	500.21	500.09	500.18	500.33	500.17	500.21	500.10
10	555.10	555.13	555.22	555.30	555.25	555.15	554.98
11	610.00	610.07	610.04	610.29	610.15	610.09	609.93
12	664.93	665.05	665.03	665.30	665.14	665.13	664.98
13	719.96	720.15	720.13	720.20	720.04	720.11	719.98

	8	9	10	11	12	13
1	60.36	60.26	60.32	60.30	60.29	60.29
2	115.26	115.29	115.32	115.25	115.22	115.22
3	170.33	170.30	170.33	170.13	170.24	170.17
4	225.30	225.20	225.26	225.17	225.11	225.32
5	280.29	280.20	280.24	280.18	280.25	280.33
6	335.29	335.22	335.21	335.14	335.17	335.29
7	390.18	390.11	390.17	390.06	390.15	390.24
8	445.22	445.11	445.18	445.17	445.14	445.29
9	500.15	500.13	500.25	500.13	500.09	500.22
10	554.98	555.04	555.18	555.03	555.06	555.29
11	610.09	609.99	610.03	609.99	609.92	610.17
12	665.04	665.00	664.93	664.89	664.92	665.13
13	720.04	719.93	719.87	719.93	719.98	720.20

Table 7.5: SWP True Reseau Positions in X Direction

	1	2	3	4	5	6	7
1	74.41	130.48	186.50	242.55	298.45	354.51	410.65
2	74.41	130.45	186.45	242.51	298.50	354.53	410.68
3	74.36	130.42	186.50	242.51	298.50	354.51	410.69
4	74.41	130.49	186.52	242.50	298.53	354.60	410.68
5	74.41	130.51	186.50	242.51	298.53	354.57	410.70
6	74.41	130.41	186.45	242.45	298.50	354.50	410.68
7	74.44	130.44	186.52	242.48	298.53	354.57	410.70
8	74.41	130.34	186.45	242.38	298.46	354.48	410.68
9	74.41	130.35	186.43	242.38	298.42	354.50	410.69
10	74.40	130.32	186.40	242.37	298.42	354.51	410.63
11	74.39	130.30	186.36	242.29	298.35	354.41	410.58
12	74.36	130.36	186.42	242.44	298.43	354.54	410.65
13	74.39	130.37	186.40	242.38	298.41	354.51	410.63

	8	9	10	11	12	13
1	466.57	522.65	578.60	634.61	690.55	745.80
2	466.61	522.71	578.60	634.68	690.61	745.87
3	466.61	522.69	578.64	634.64	690.65	746.08
4	466.63	522.71	578.66	634.51	690.63	746.10
5	466.64	522.71	578.71	634.58	690.63	746.19
6	466.60	522.66	578.64	634.50	690.61	746.26
7	466.67	522.75	578.67	634.55	690.55	746.31
8	466.61	522.73	578.63	634.50	690.44	746.24
9	466.60	522.69	578.66	634.50	690.42	746.29
10	466.57	522.69	578.66	634.43	690.39	746.29
11	466.53	522.57	578.53	634.33	690.25	746.26
12	466.61	522.68	578.60	634.50	690.23	746.40
13	466.60	522.68	578.62	634.54	690.38	746.49

Table 7.6: SWP True Reseau Positions in Y Direction

	1	2	3	4	5	6	7
1	54.43	54.34	54.32	54.41	54.34	54.36	54.32
2	110.45	110.32	110.55	110.55	110.49	110.51	110.44
3	166.38	166.39	166.49	166.68	166.49	166.54	166.36
4	222.47	222.48	222.68	222.72	222.68	222.57	222.50
5	278.52	278.46	278.70	278.77	278.66	278.70	278.55
6	334.61	334.54	334.74	334.74	334.72	334.62	334.53
7	390.63	390.56	390.73	390.82	390.72	390.63	390.54
8	446.61	446.66	446.75	446.92	446.87	446.85	446.64
9	502.86	502.73	502.83	502.99	502.82	502.86	502.75
10	558.83	558.85	558.95	559.04	558.98	558.88	558.70
11	614.81	614.88	614.85	615.10	614.96	614.89	614.74
12	670.82	670.93	670.91	671.19	671.03	671.01	670.86
13	726.92	727.12	727.09	727.16	727.01	727.08	726.94

	8	9	10	11	12	13
1	54.39	54.29	54.34	54.33	54.32	54.32
2	110.37	110.39	110.42	110.35	110.32	110.32
3	166.52	166.49	166.52	166.31	166.42	166.35
4	222.57	222.45	222.52	222.43	222.37	222.58
5	278.63	278.53	278.57	278.52	278.59	278.67
6	334.71	334.64	334.62	334.55	334.58	334.71
7	390.68	390.61	390.66	390.55	390.65	390.73
8	446.80	446.68	446.75	446.74	446.71	446.87
9	502.80	502.78	502.90	502.78	502.73	502.87
10	558.70	558.77	558.91	558.76	558.78	559.02
11	614.89	614.79	614.83	614.79	614.72	614.97
12	670.93	670.89	670.82	670.77	670.80	671.01
13	727.01	726.89	726.82	726.89	726.94	727.16

Figure 7.1. This figure shows the amount by which each pixel in the low-dispersion SI must be shifted along the dispersion direction from its original uncorrected position in order to achieve a linear dispersion solution. This correction is applied uniformly throughout the spatial direction of the image so that entire image columns (i.e., lines of constant wavelength) are shifted by the same amount.

In high dispersion, since the vectors which correct for wavelength nonlinearities are determined separately for each order, the corrections for each order are applied in a “block-like” fashion. That is, each pixel in a line of constant wavelength for a given order is shifted by the same amount. The starting and ending spatial positions for each “block” about an order are set halfway between the adjacent orders.

## 7.2 Additional Corrections for Low Dispersion

### 7.2.1 Aperture Alignment

The low-dispersion SI includes the spectral data for both the large and small apertures. Because the centers of the two apertures are not aligned along a line of constant wavelength in the rotated image space, it would be impossible to have a single dispersion solution apply to the entire image. Therefore, a shift along the dispersion direction is introduced for the small-aperture spectra so that both apertures are on a common wavelength scale. The small-aperture data for SWP are shifted by 0.8 pixels in the dispersion direction towards longer wavelengths, and for LWP and LWR the small-aperture data are shifted by 2.3 pixels towards shorter wavelengths. The shift is applied uniformly to all pixels within the small-aperture region of the low-dispersion SI, which is defined to extend from row 1 through row 33 of the image.

### 7.2.2 Wiggle Corrections

The LWP and LWR cameras are known to exhibit localized discontinuities in the spectral format which are believed to be due to slight misalignments between neighboring fiber optic bundles in the output stage of the ultraviolet converter (UVC) portion of the cameras. These misalignments are seen as abrupt changes in the spatial centroid of the spectrum of up to 1 pixel. In addition to these abrupt changes, there also exist more slowly varying “wiggles” in the spectral format. These wiggles can have peak-to-peak amplitudes of 1 pixel or more within the space of a few dozen pixels along the dispersion direction. Figures 7.2 and 7.3 show the locations of the spectral centroid as a function of wavelength for the LWP and LWR cameras, respectively. Note the sharp discontinuities at  $\sim 3290\text{\AA}$  in the large aperture (the feature at  $\sim 3100\text{\AA}$  is a reseau) and at  $\sim 2780\text{\AA}$  and  $\sim 3290\text{\AA}$  in the small aperture for the LWP. The LWR shows similar discontinuities at  $\sim 2450\text{\AA}$  and  $\sim 2830\text{\AA}$  in the large aperture. The existence of these wiggles complicates the task of spectral extraction since it is necessary to have the extraction slit follow the changing spectral centroid in order to ensure that all of the spectral flux is extracted at a given wavelength.

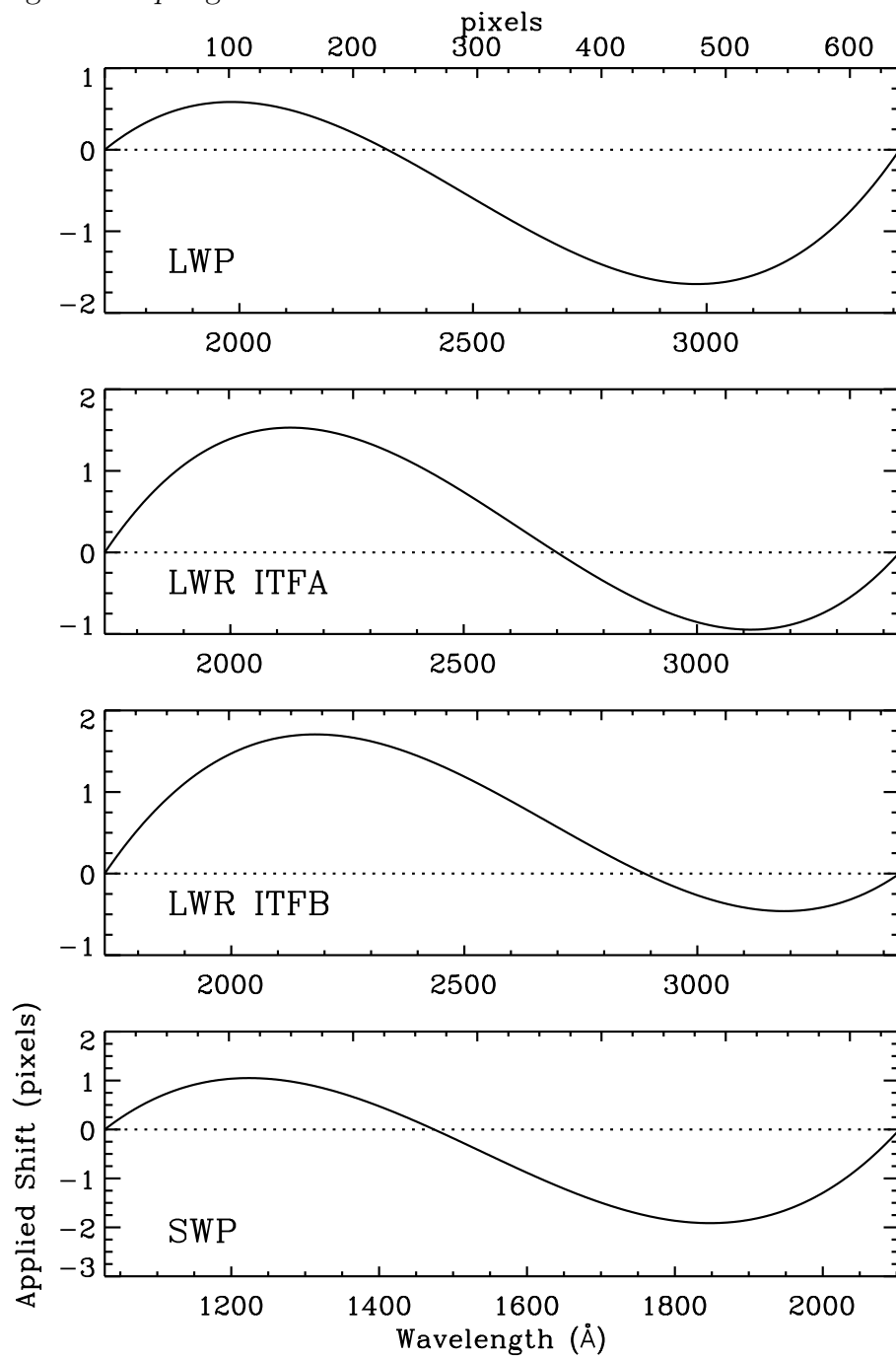


Figure 7.1: Low-dispersion wavelength linearization correction vectors.

To compensate for these wiggles, the spectral centroid as a function of wavelength has been measured from approximately 30 low-dispersion SI for each of the LWP and LWR cameras and the average deviations have been incorporated into the resampling step of the image processing system as an additional geometric correction vector. These corrections affect only the spatial dimension of the low-dispersion SI. Separate deviation vectors are applied for the large- and small-aperture regions of the LWP and LWR low-dispersion SI. As Figures 7.2 and 7.3 show, the deviation vectors for the two apertures are qualitatively similar, but differ in detail, due to the fact that they are imaged onto different portions of the camera faceplate. Figures 7.4 and 7.5 show examples of the measured centroid locations for “dewiggled” versions of LWP and LWR images.

### 7.2.3 Large-Aperture Tilt Correction

The major axis of the large aperture in low-dispersion data is not precisely perpendicular to the direction of dispersion. The major axis is at an angle, called the  $\omega$  angle, with the dispersion direction, which is slightly different for each of the three cameras. The geometry of the entrance apertures in relation to the image scan lines and dispersion directions as they appear in the low-dispersion SI is shown in Figure 7.6. The left side of each figure shows the intrinsic geometry with no corrections applied, the middle portion shows the resulting geometry after applying the aperture alignment correction only, and the right side shows the results after applying both alignment and tilt corrections. Note that the major axis of the large aperture in high-dispersion data is very nearly coincident with the direction of dispersion so no tilt correction is necessary.

The error introduced by extracting extended spectral data (data that fills the large aperture) which has not been tilt corrected, by summing the flux perpendicular to the dispersion can be estimated as follows. The maximum tilt of the large aperture with respect to the dispersion direction occurs in the SWP camera, with an  $\omega$  angle of  $81^\circ$ . If the length of the large aperture is taken to be 14.2 pixels (based on a plate scale factor of 1.53 arcsec/pixel), then the displacement from the line perpendicular to the dispersion direction is 1.1 pixels at each end of the aperture, or approximately  $1.9\text{\AA}$ . Spectral features will show some broadening if extracted perpendicular to the dispersion ( $\omega = 90^\circ$ ), which will amount to a broadening of the base of the point spread function by  $3.8\text{\AA}$ . The overall effect is in reality not as severe as a simple convolution of the data with a  $3.8\text{\AA}$  wide slit, because the part of the signal extracted near the slit center is not really being degraded. A more precise approximation to the error is to think of the  $10\text{\AA}$  slit width as being convolved with a triangular function with FWHM of  $2\text{\AA}$  and a base width of  $4\text{\AA}$ , which will result in a degradation in resolution of 20–25%.

Since this is a significant effect, a correction is made to “detilt” the large-aperture data for observations that result in the detection of spatially extended spectra. This correction is obviously not necessary for point source spectra, nor is it appropriate for most trailed or multiple observations because in these types of observations the source is moved along the FES x-axis which is nearly perpendicular to the dispersion direction. Multiple spectra acquired

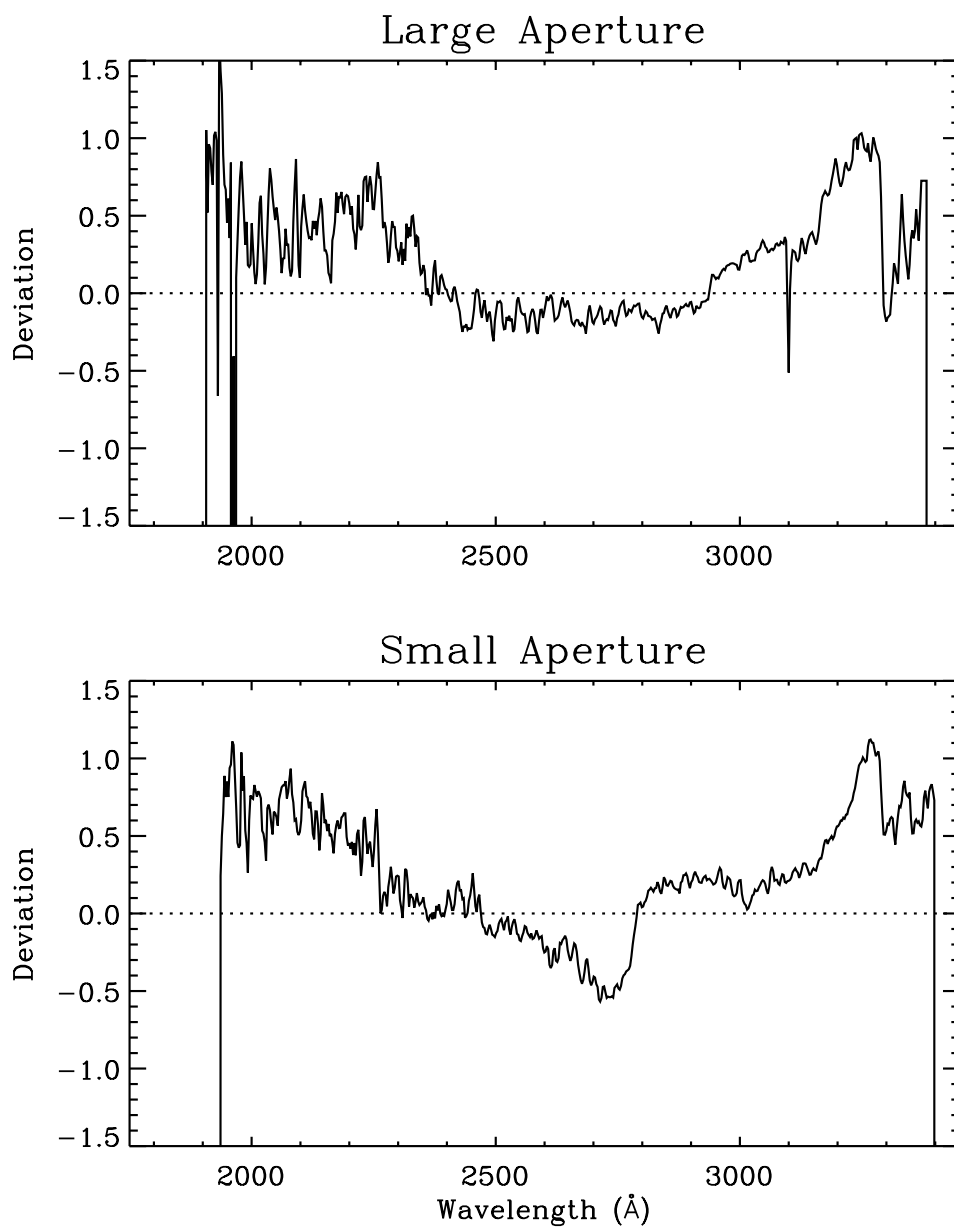


Figure 7.2: Spectrum centroid location in LWP low-dispersion SI data.

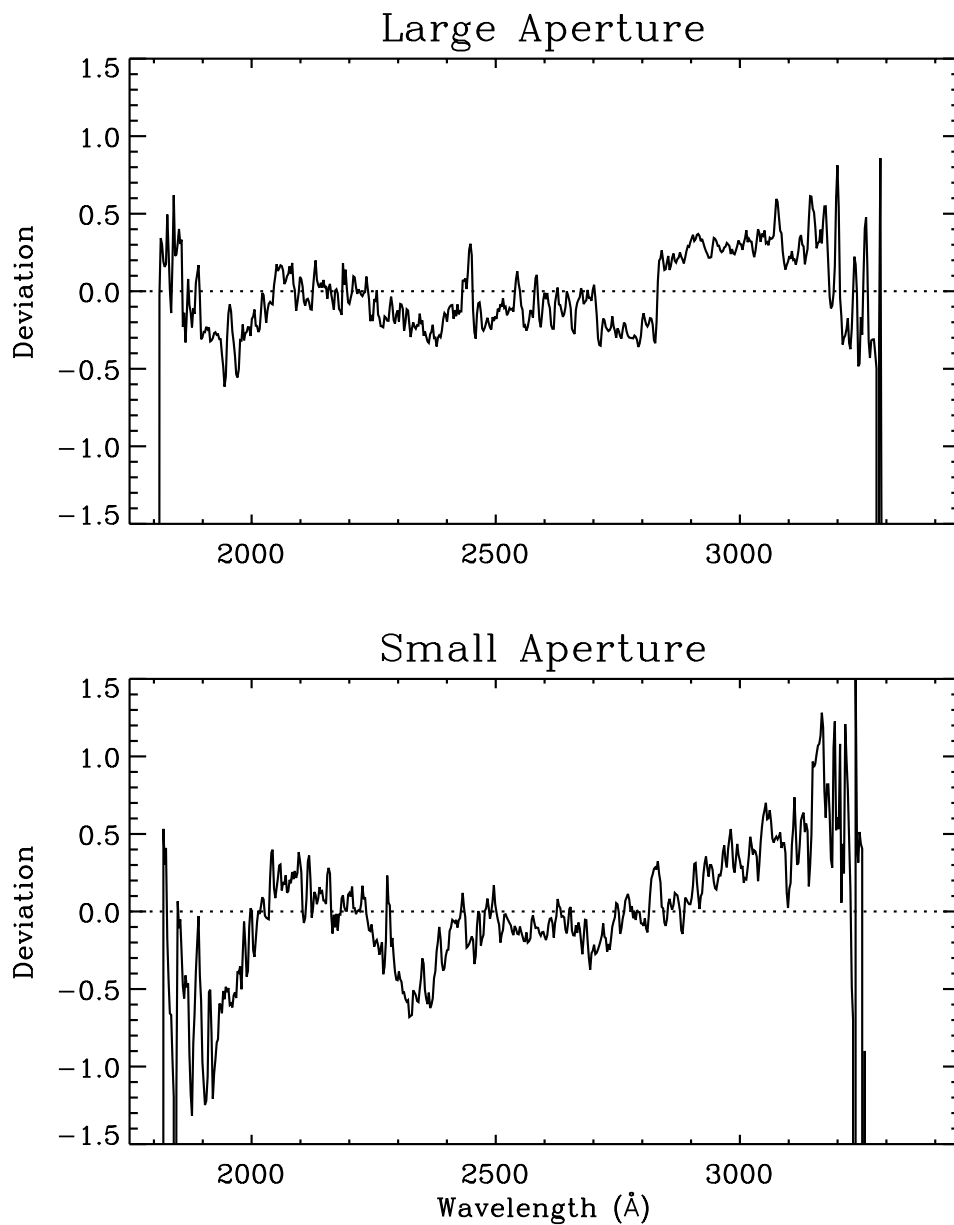


Figure 7.3: Spectrum centroid location in LWR low-dispersion SI data.

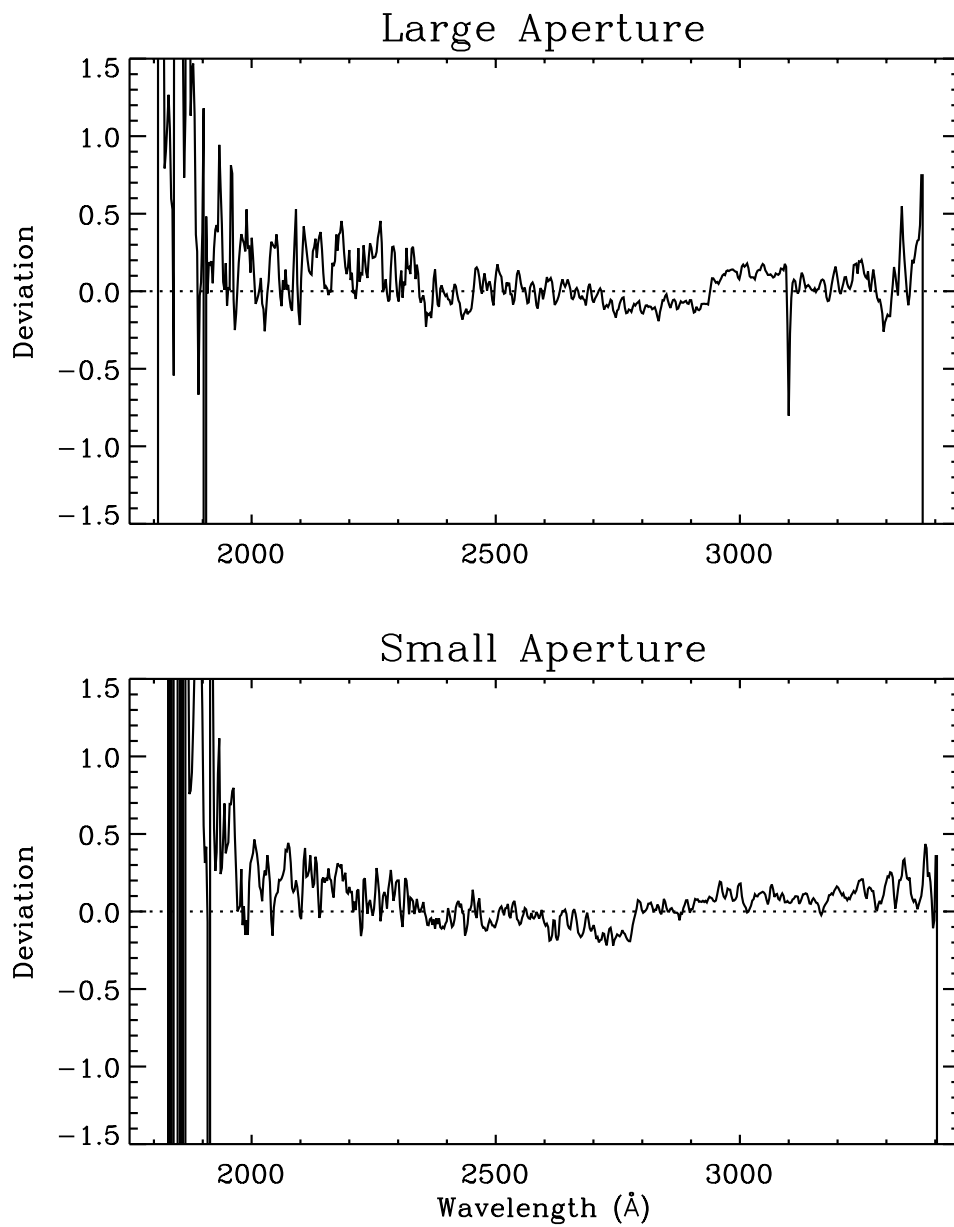


Figure 7.4: Spectrum centroid location in “dewiggled” LWP low-dispersion SI data.

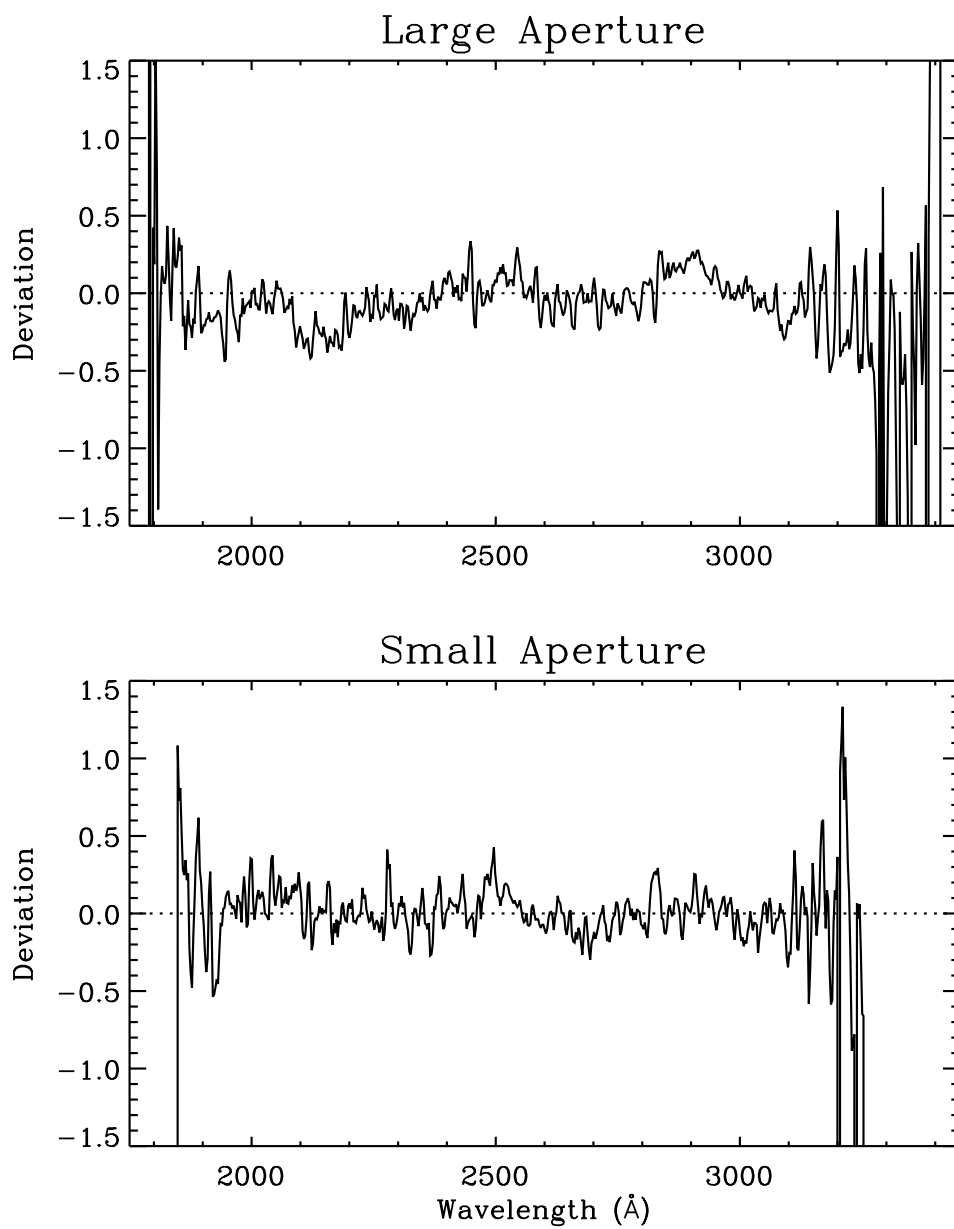


Figure 7.5: Spectrum centroid location in “dewiggled” LWR low-dispersion SI data.

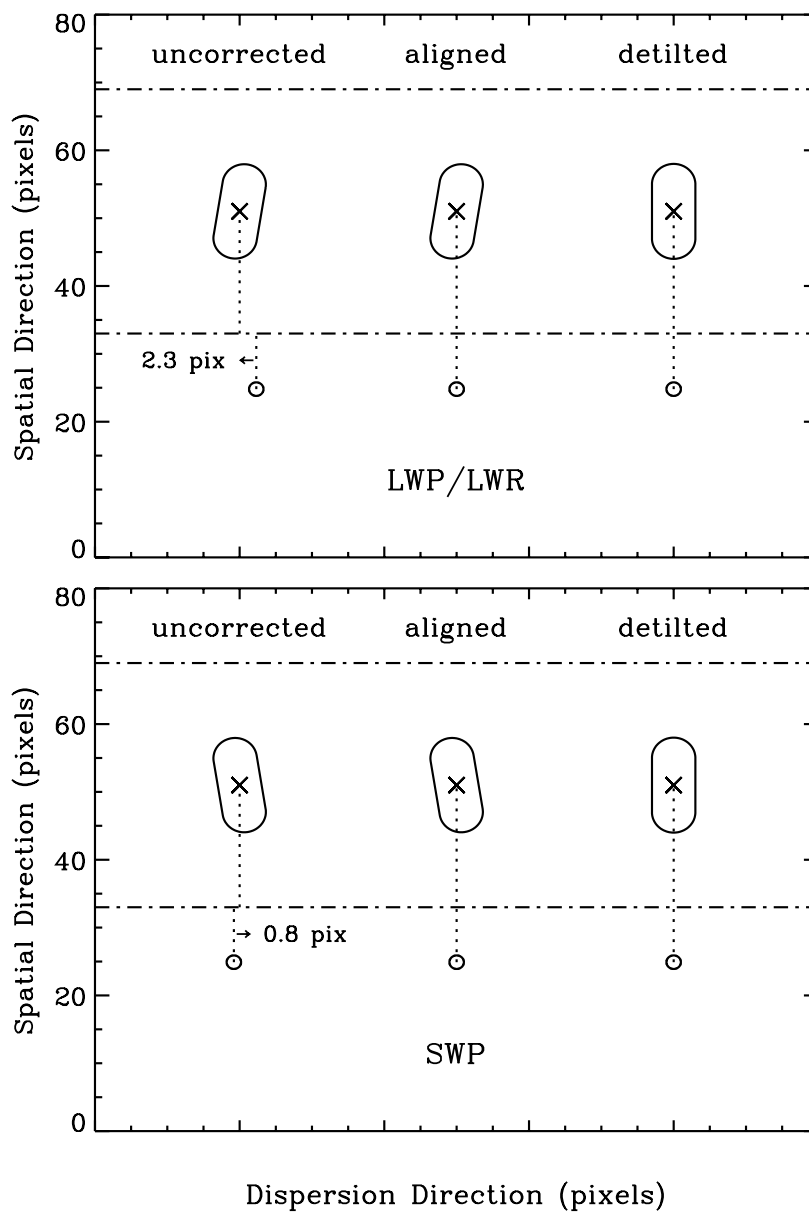


Figure 7.6: Geometry of the spectrograph apertures as they appear in the low-dispersion SI.

along the major axis of the aperture, however, are tilt corrected. The tilt correction is not applied to any non-multiple spectrum having object class designation 10–57 (stellar sources), regardless of whether the spectrum is determined to be point or extended. Presumably a stellar spectrum measured to be extended is saturated.

The tilt correction is only applied to a region of the low-dispersion SI that extends for 18 image lines on either side of the predicted center of the large aperture, thus leaving the small-aperture data intact. The extent of the correction region was chosen so as to include the areas on either side of the aperture which are used for background subtraction in the subsequent extraction step of the image processing. The actual correction is accomplished by simply shifting each image line in the dispersion direction by an amount given by:

$$\Delta x = \Delta y \times \tan(\omega_t)$$

where  $\Delta y$  is the number of spatial image lines between the center of the large aperture and the image line under consideration, and  $\omega_t$  is the tilt angle of the aperture. Note that this correction is a projection of the aperture onto the spatial axis of the image, as opposed to a rotation about the center of the aperture, since the latter would result in a slight remapping of the spatial character of the data.

## 7.2.4 Wavelength and Spatial Normalization

As discussed in Chapter 8.1, global shifts in the location of the spectral format occur as a function of time and camera temperature. These global movements of the spectral format appear as displacements of the spectrum in both the spatial and dispersion directions of the low-dispersion SI. The resulting change in the starting wavelength (i.e., the wavelength value assigned to column 1 of the low-dispersion SI) can be compensated for through the application of zeropoint corrections derived from wavelength calibration (WAVECAL) images (Chapter 8.1). While this would result in the assignment of the correct wavelength zeropoint for each low-dispersion SI, it would also result in the assignment of a *different* starting wavelength for each image. Having spectra with offset wavelength scales would affect subsequent data analysis.

To alleviate this effect in low dispersion, zeropoint shifts in both the spatial and dispersion directions are applied to the image resampling vectors so that all spectra for a given camera have the same starting wavelength and the same spatial location within the low-dispersion SI. Furthermore, additional shifts are applied to the image resampling vectors so that both long wavelength cameras provide coverage of the same spectral range. The spatial centroid of large-aperture spectra is chosen to lie on or about line 51 of the low-dispersion SI for all cameras. The resulting centroid of small-aperture spectra is approximately at line 25. Due to the nature of the LWP geometry, this requires an additional adjustment to the LWP data in order to place the large-aperture spectrum at the top of the file. The common wavelength starting values are 1050Å and 1750Å for the short and long wavelength cameras, respectively. The amount of the zeropoint shift to be applied to each image is computed from the difference between the desired starting wavelengths and those predicted from the time-

and temperature-corrected dispersion constants (Chapter 8.1). Image-to-image scatter in the precise location of the spectral format leads to 1-sigma errors in the predicted wavelength and spatial zeropoints of  $\sim 0.3\text{\AA}$  and 0.26 pixels, respectively, for the SWP and  $\sim 0.6\text{\AA}$  and 0.35 pixels, respectively, for the LWP.

## 7.3 Additional Corrections for High Dispersion

### 7.3.1 Order De-splaying

The differential rotation (“splaying”) of individual echelle orders results from the combined effects of the echelle and cross-dispersing elements. The ratio of these two components of dispersion is proportional to the ratio of the grating orders and can be expressed as  $1/m_{echelle}$  times a constant. The change in this ratio from one order to the next causes the orders to be differentially rotated (“splayed”) on the detector. The de-splaying angle for each camera was determined after first rotating the raw space image in the *GEOM* module and recognizing conceptually that the  $y$  coordinate of the rotated image may be replaced with the parameter  $1/m_{ech}$ . Since the  $y$  positions of the orders are distributed as  $1/m_{ech}$ , this axis may be thought as mapping a continuous (floating-point) parameter,  $1/m_{ech}$  (Smith 1990a, 1990b). A single differential rotation constant may then be incorporated which is used ultimately to detilt each of the  $y$  pixel-lines with respect to a reference (“horizontal”) line position. This detilting is in fact a de-splaying of each of the lines in the image with respect to a reference order: a single constant which properly takes into account the variation of the splaying-tilt with  $m_{ech}$  across the image field. The de-splaying angle is determined empirically and by means of a virtual-coordinate artifice rather than from grating parameters of the spectrograph because *NEWSIPS* does not yet “know” what  $m_{ech}$  value will correspond to each  $y$  line in the rotated raw-image space in which the de-splaying corrections are computed. The de-splaying correction performed in *NEWSIPS* processing is such that pixels which lie along “central”  $x$ - $y$  axes (positioned about the center of the target area) have no correction applied. Pixels which lie off of the “central” axes have a de-splaying correction applied that is directly proportional to the displacement of the pixel’s position from the origin of the “central” axes. The de-splaying correction corresponds to a shift in the  $y$  (i.e., line) direction only.

Determination of the splaying constants was done iteratively for a collection of continuum images for each camera until values were found which forced all the orders to fall along constant pixel lines. In practice, the “wiggles” of the orders (Chapter 7.3.3) limited the accuracy to which the de-splaying constants could be determined. However, small residual errors in these constants were presumed to be incorporated as residual slopes in the wiggle vectors.

### 7.3.2 Wavelength and Spatial Normalization

Displacement vectors that adjust for the spatial shifting of the orders with respect to a fiducial image are generated during the raw image screening process and applied to science

images during the *GEOM* stage. These vectors include a global shift of each image and, if needed, differential order shifts. A detailed discussion of the order registration process can be found in Chapter 4.9.

Note that unlike the low-dispersion counterpart, no starting wavelength normalization correction is applied to high-dispersion data. As a result, a resampling of individual spectra to a common wavelength scale is in general required to coadd properly multiple high-dispersion images of a given source.

### 7.3.3 Wiggle Corrections

Localized discontinuities (wiggles) in the spatial direction are also detectable in high-dispersion images for all three cameras. Corrections, similar to those developed in low dispersion for the long-wavelength cameras, have been derived which map out these distortions present in every order. The SWP wiggles demonstrate a time dependency in patchy areas on the camera surface. Therefore, two SWP correction templates have been derived: one for early-epoch (before 1988 January 02) images, the other for late-epoch (after 1990 January 02) data. Wiggle corrections are interpolated linearly for SWP high-dispersion images obtained between these two dates. The LWP and LWR cameras have only single-epoch correction templates. The wiggles among the SWP images correlate well enough that a mean-wiggle template removes at least half the amplitude of the excursions in an individual image. The wiggles present in long-wavelength images are not as well correlated.

## 7.4 Flux Resampling Algorithm

The final coordinate mapping is derived by adding the individual geometric corrections in a vectorial fashion. Consequently, the transformation from raw image space to geometrically rectified space necessitates the use of a sophisticated resampling algorithm because the raw image pixels must be resampled from the irregular grid resulting from the vector mapping to a regular grid to produce the SI. This type of two-dimensional interpolation is mathematically challenging and particularly difficult to solve satisfactorily. The intensity values (FNs) in the LI are resampled to the geometrically corrected space of the SI using a modified Shepard method, an algorithm found in the NAG (1990) library. The interpolant for the modified Shepard method is continuous and also possesses first derivative continuity. The method is local in that the output flux value is dependent only upon data in a surrounding neighborhood.

## 7.5 Data Quality ( $\nu$ ) Flag Resampling

Since the intensity values are resampled in the mapping from the raw space of the LI to the geometrically rectified space of the SI, the  $\nu$  flag values must also be appropriately mapped into this new space. In order to map the flag values from raw space to the new geometric

space, a “resampling” algorithm is clearly *not* desired as the  $\nu$  flags have a very specific discrete meaning which must be maintained. The flag values need to be mapped to their new coordinates such that they retain their initial values, but also are appropriately assigned to additional locations in the remapped space in accordance to the distribution of intensities.

The residuals from integer coordinates are computed for the sample and line final floating-point geometric coordinates. These residuals are then evaluated in combination against a pre-defined threshold of 0.25. This threshold represents an “in-between” region which determines if the  $\nu$  flags should be mapped to 1, 2, 3, or 4 pixels in the final geometric space.

## 7.6 High-Dispersion Cosmic Ray Detection Algorithm (*COSMIC\_RAY*)

This algorithm initially was developed to flag off-order (i.e., background) pixels that are potentially affected by a cosmic ray event. The cosmic ray flagging procedure was conceived for application by the high-dispersion background determination (*BCKGRD*) module.

The flagging by the *COSMIC\_RAY* module is done by dividing the non-illuminated regions of the target into  $57 \times 57$ -pixel boxes and computing local means and rms statistics for each box (see Fahey, Bogert, and Smith 1994). A flagging-threshold was determined empirically as a function of a normalized rms parameter (rms/mean) for each camera. The choice of this criterion was driven by a trade-off between requirements of detecting the “coma” of cosmic rays and not triggering on high points in the background regions when the rms is large.

The sensitivity of the *BCKGRD* solutions to cosmic rays actually is caused by the surrounding low-level coma regions of these central “hit” areas. This can cause ringing over a larger spatial scale across the image. In practice it was difficult to discriminate against the background-flux granularity without sacrificing the *COSMIC\_RAY* module’s ability to detect coma regions. An optimization of the trade-off between detecting low-level coma and not flagging isolated high pixels was such that the flagging still occurred frequently enough that instabilities, resulting from pixel-undersampling, occurred in many background extractions for all three cameras. As a result, the cosmic ray image extension to the high-dispersion SI (CRHI) is not used by *BCKGRD* but is retained as an output product for informational purposes only. The contents of the CRHI are encoded as follows. Pixels which are masked out by the *COSMIC\_RAY* module (e.g., on-order pixels and regions outside the target area) are denoted in the CRHI with a value of +64. Non-condition pixels (i.e., those that are not flagged as cosmic rays) are signified in the CRHI by a value of +32. Pixels that are determined to be affected by cosmic rays are indicated with a value of +160.

## 7.7 GEOM Output

### 7.7.1 Low-Dispersion

The low-dispersion SI and VD FITS files (SILO and VDLO, respectively) are the main output data products produced during the image resampling stage. The SILO contains the geometrically resampled intensity data and the resampled  $\nu$ -flag image corresponding to the intensity data. The intensity data are output as a FITS primary array, and the associated  $\nu$  flags are output as the corresponding FITS image extension. The VDLO contains the summation of all the geometric corrections implemented to perform the single image resampling and gives, for each pixel in LI space, the final  $x$  and  $y$  coordinate in SI space stored in a FITS primary array. As discussed in Chapter 5, the raw cross correlation data are retained in a FITS binary table extension of the VDLO.

The *GEOM* module writes the following information to the HISTORY portion of the low-dispersion image label:

- four Chebyshev coefficients used to define the wavelength linearization,
- tilt angle (applied only to extended sources),
- wavelength zeropoint and spatial shifts,
- final time/temperature corrected dispersion constants, and
- predicted center line of the large and small apertures.

### 7.7.2 High-Dispersion

The high-dispersion SI and VD FITS files (SIHI and VDHI, respectively) are the main output data products produced during the image resampling stage. The SIHI contains the geometrically resampled intensity values stored in a FITS primary array, the resampled  $\nu$ -flag image corresponding to the intensity data stored as a FITS image extension, the associated starting wavelength, wavelength increment, and predicted and found line positions for every order stored in a FITS binary table extension, and an array of pixels which have been flagged as cosmic rays by the high-dispersion *COSMIC.RAY* module stored as a FITS image extension. The VDHI contains the summation of all the geometric corrections implemented to perform the single image resampling and gives, for each pixel in LI space, the final  $x$  and  $y$  coordinate in SI space stored in a FITS primary array. As discussed in Chapter 5, the raw cross correlation data are retained in a FITS binary table extension of the VDHI.

The following information is written to the HISTORY portion of the high-dispersion image label by the *GEOM* module:

- epoch of the spatial deviation (wiggle) file,
- de-splaying angle in radians, and

- predicted line center of a representative “checkpoint” echelle order (order 100 for SWP or order 90 for the LWP and LWR). The LWP processing HISTORY initially reported the line position for order 100. This was subsequently changed to order 90 after the start of the processing effort, as this order is in a region of higher sensitivity than order 100 for the LWP and LWR. This change only affects LWP and LWR high-dispersion images processed after July 28, 1997.

## 7.8 *COSMIC\_RAY* Output

The following information is written to the HISTORY portion of the high-dispersion image label by the *COSMIC\_RAY* module:

- mean FN of interorder background and
- number of flagged pixels.